

Spatial Distribution of the Galactic Center Diffuse X-Rays and the Spectra of the Brightest 6.4 keV Clumps

Katsuji KOYAMA, Yojiro TAKIKAWA, Yoshiaki HYODO, Tatsuya INUI, Masayoshi NOBUKAWA, Hironori MATSUMOTO and Take
Department of Physics, Graduate school of Science, Kyoto University, Sakyo-ku, Kyoto 606-8502
koyama@cr.scphys.kyoto-u.ac.jp

(Received ; accepted)

Abstract

The high energy resolution and low background, particularly in the hard X-ray band, of the X-ray Imaging Spectrometer onboard Suzaku provide excellent spectra of the Galactic center diffuse X-rays (GCDX). This paper reports on the results of spatially resolved spectroscopy of GCDX. The most pronounced features of GCDX are the K-shell transition lines from neutral (FeI) and He-like (FeXXV) irons at energies of 6.4 keV and 6.7 keV, respectively. The fluxes of these lines are non-uniformly and asymmetrically distributed with respect to Sgr A*. The 6.4 keV lines are particularly bright on the positive side of the Galactic longitude (east-side) with clumpy structures. A bright clump near the GC exhibits a time variability over a timescale of a few years. Neither the 6.4 keV nor 6.7 keV line flux shows close proportionality to the continuum flux (5–10 keV band); the 6.4 keV line shows excess on the high flux side, and vice versa for the 6.7 keV line. On the other hand, the sum of the 6.4 keV plus 6.7 keV line fluxes with a ratio of 1:2 shows good proportionality to the continuum flux, and hence we phenomenologically decomposed the continuum flux of the GCDX into the 6.4 keV- and 6.7 keV-associated continuums with a flux ratio of 1:2. Based on these facts, we have tried to estimate the contribution of diffuse and integrated flux of point sources to the GCDX.

Key words: Galaxy: center—ISM: supernova remnant —X-ray spectra

1. Introduction

The Galactic center diffuse X-rays (GCDX) exhibit many K-shell lines from highly ionized atoms, such as the $K\alpha$, $K\beta$ and $K\gamma$ lines of He-like (FeXXV) and H-like (FeXXVI) iron, and the $K\alpha$ line from He-like nickel (NiXXVII) (e.g. Koyama et al. 2007d). These K-shell lines carry key information about the plasma physics. The electron and ionization temperatures of a hot plasma are constrained by the line flux ratio of FeXXV- $K\beta$ to FeXXV- $K\alpha$ and that of FeXXVI- $K\alpha$ to FeXXV- $K\alpha$, respectively. Koyama et al. (2007d), using these line ratios, reported that the 5–11.5 keV band spectrum of the GCDX is naturally explained by a 6.5 keV-temperature plasma in collisional ionization equilibrium (CIE) plus a power-law component with a photon index of $\Gamma=1.4$. The former component has nearly the same flux as that from the latter component (see figure 7, in Koyama et al. 2007d). The origins of these components and highly ionized atomic lines are, however, open questions.

In addition to these highly ionized atomic lines, the $K\alpha$ and $K\beta$ lines from neutral irons (FeI) and the $K\alpha$ line from neutral nickels (NiI) have also been discovered. A likely origin of these neutral K-shell lines is due to fluorescence irradiated by external X-ray sources (e.g. Koyama et al. 1996; Murakami et al. 2000; Murakami et al. 2001; Koyama et al. 2007b; Koyama et al. 2008; Nobukawa et al. 2008). However, alternative scenarios, such as a bombarding of energetic electrons, have also been proposed (e.g. Predehl et al. 2003; Wang et al. 2006; Yusef-

Zadeh et al. 2007).

The key questions are: what are the origins of the 6.7 keV and 6.4 keV lines, and how much is the contribution of unresolved point sources? The 6.7 keV and 6.4 keV lines in the GCDX are spatially and spectrally entangled with each other. Spatially resolved spectroscopy could disentangle this complicated situation. Together with good energy resolution and low background near and above the ~ 6 keV band, Suzaku (Mitsuda et al. 2007) is the best satellite to date for this study. This paper focuses on the 5–11.5 keV band X-rays in the sub-degree region near the Galactic center (GC). The distance to GC is assumed to be 8 kpc (Reid 1993). In this paper, quoted errors are at the 90% confidence level, unless otherwise mentioned. We use the Galactic coordinates; hence, the east means the positive Galactic longitude side and vice versa for the west.

2. Observations and Data Reduction

Two pointing observations (here, the east and west fields) towards GC were performed in September of 2005, with the X-ray Imaging Spectrometers (XIS; Koyama et al. 2007a), at the focal planes of the X-Ray Telescopes (XRT; Serlemitsos et al. 2007) onboard the Suzaku satellite (Mitsuda et al. 2007). The data-selection criteria and subtraction method of the non X-ray background (NXBG) are the same as those given in Koyama et al. (2007d). The charge transfer inefficiency (CTI) and fine gain-tuning of CCD-to-CCD and segment-to-segment levels (for the CTI

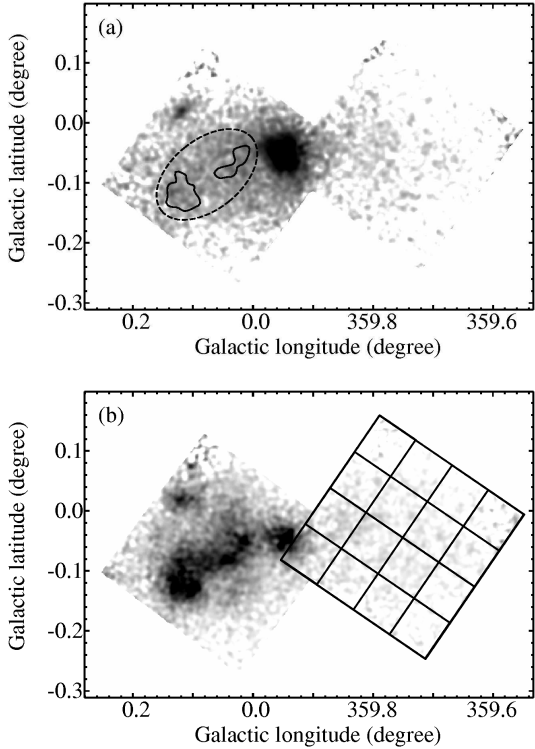


Fig. 1. Mosaic (2-pointings of the east and west fields) maps of the 6.7 keV line (a) and of the 6.4 keV line (b) bands. The east and west fields are the left (east), and the right (west) sides, respectively. Solid polygons in figure (a) are 6.4 keV clumps (here, the west clump is source 1, and the east clump is source 2), while the dashed ellipse is the background region. The background data for the 6.4 keV clumps were obtained by excluding the data of source 1 and 2. The grid in the west field shows 16 segmentations for the spatial resolved study (see text).

and the CCD segment, see Koyama et al. 2007a) were self-calibrated using the $K\alpha$ lines of Fe XXV (6.7 keV), Fe I (6.4 keV) and Helium-like sulfur (S XV) (2.46 keV). The absolute gain-tuning was made using the ^{55}Fe calibration sources irradiating the CCD corners, and also using the Fe XXVI- $K\alpha$ line, which has a relatively simple structure. The over-all systematic error of our gain determination near the iron and nickel K-shell energies is estimated to be within $^{+3}_{-6}$ eV. The details concerning the calibration procedures and the results are given in Koyama et al. (2007d).

For a timing study of the 6.4 keV line flux, we used the Chandra GC data obtained by the Advanced CCD Imaging Spectrometer array (ACIS-I) with total exposure times of ~ 500 ks. The logs are ObsID 2943, 2951, 2952, 2953, 2954, 3392, 3393, 3663 and 3665, observed in 2002. The data were reprocessed, using the CIAO version 3.4 and the calibration database version 3.4.0.

3. Analyses and Results

3.1. The Extended Emission near the GC (GCDX)

In order to see the spatial distribution of the Fe K-shell lines, we made line images of the 6.7 keV (Fe XXV- $K\alpha$)

and 6.4 keV (Fe I- $K\alpha$) lines with the respective energy bands of 6.62–6.78 keV and 6.32–6.48 keV. The images are shown in figure 1, where they include both the relevant line flux and the underlying continuum flux. From figure 1, we can see that the 6.7 keV line flux in the east field is systematically larger than that in the west field. This contrast is clearer in the 6.4 keV line band, showing clear clumps near $(l, b) = (0.03, -0.07)$ and $(0.12, -0.12)$ (source 1 and 2; the polygons in figure 1a).

To study more quantitatively, we divided both the east and west fields into 16 segments each (32 segments for total), as given by the grid in figure 1b. Since the 4 segments in each field corner are partially contaminated by the calibration X-rays (Mn I- $K\alpha$ and $K\beta$ lines at 5.9 and 6.5 keV, respectively), we made the X-ray spectra for the remaining 24 segments in the 5–11.5 keV band, and fitted with a phenomenological model as follows:

$$\text{Abs} \times (\text{PL} + \text{Abs} \times \text{CXB} + \text{Gaussians}) \quad [\text{photons keV}^{-1} \text{ cm}^{-2} \text{ s}^{-1} \text{ str}^{-1}], \quad (1)$$

where PL is a power-law function, $\text{PL} = A \times E^{-\Gamma}$. CXB is the cosmic X-ray background modeled as $\text{CXB} = 8.75 \times (E/1 \text{ keV})^{-1.486}$. Abs is the intra-Galactic absorption in the line of sight to the GC, and is given by $e^{-\sigma(E)N_{\text{H}}}$, where N_{H} and $\sigma(E)$ are, respectively, the hydrogen column density and the absorption cross section with the solar abundances. The GCDX suffers due to the Galactic absorption (Abs) on the front side of the GC, while the CXB suffers due to both (front and back) side absorptions; hence, Abs is applied twice to the CXB, as is explicitly given in equation 1. Gaussians are given as $(F/\sqrt{2\pi}w)e^{-(E-E_{\text{C}})^2/2w^2}$, where w is the intrinsic line width (1σ).

Following Koyama et al. (2007d), we employed 10 K-shell lines (10 Gaussians) due to highly ionized and neutral atoms. The brightest 4 lines are $K\alpha$ from neutral (Fe I), He-like (Fe XXV) and H-like (Fe XXVI) irons and $K\beta$ of Fe I, at 6.4, 6.7, 6.97 and 7.06 keV, respectively. The other weak lines are $K\alpha$ from neutral (Ni I) and He-like (Ni XXVII) nickel, $K\beta$ and $K\gamma$ from Fe XXV and Fe XXVI, at 7.47, 7.81, 7.88, 8.25, 8.29, and 8.70 keV, respectively.

At first, we fitted the spectra from the full region of the east and west fields separately, with essentially the same fitting procedures as those of Koyama et al. (2007d): the line center energy, width and normalization (flux) of Fe I- $K\beta$ are fixed to 1.103, 1.103 and 0.11 times to those of Fe I- $K\alpha$ (see Koyama et al. 2007d). The widths (w) for the 6 weak lines were fixed to be 1 eV (narrow line approximation). Then, using the best-fit line widths (w) and the line center energies (E_{C}), we fitted the 24-segment spectra. The line flux ratio of Fe I- $K\beta$ /Fe I- $K\alpha$ was fixed to the theoretical value of 0.11 (see Koyama et al. 2007d). Therefore, the free parameters are normalizations of the power-law component (A) and those of the emission lines (F) except for Fe I- $K\beta$, N_{H} and the power-law index (Γ).

Using the best-fit photon indices (Γ), the line fluxes of 6.4 keV ($F_{6.4}$) and 6.7 keV ($F_{6.7}$), the energy flux in the 5–10 keV band (L_{5-10}), and the equivalent widths of the

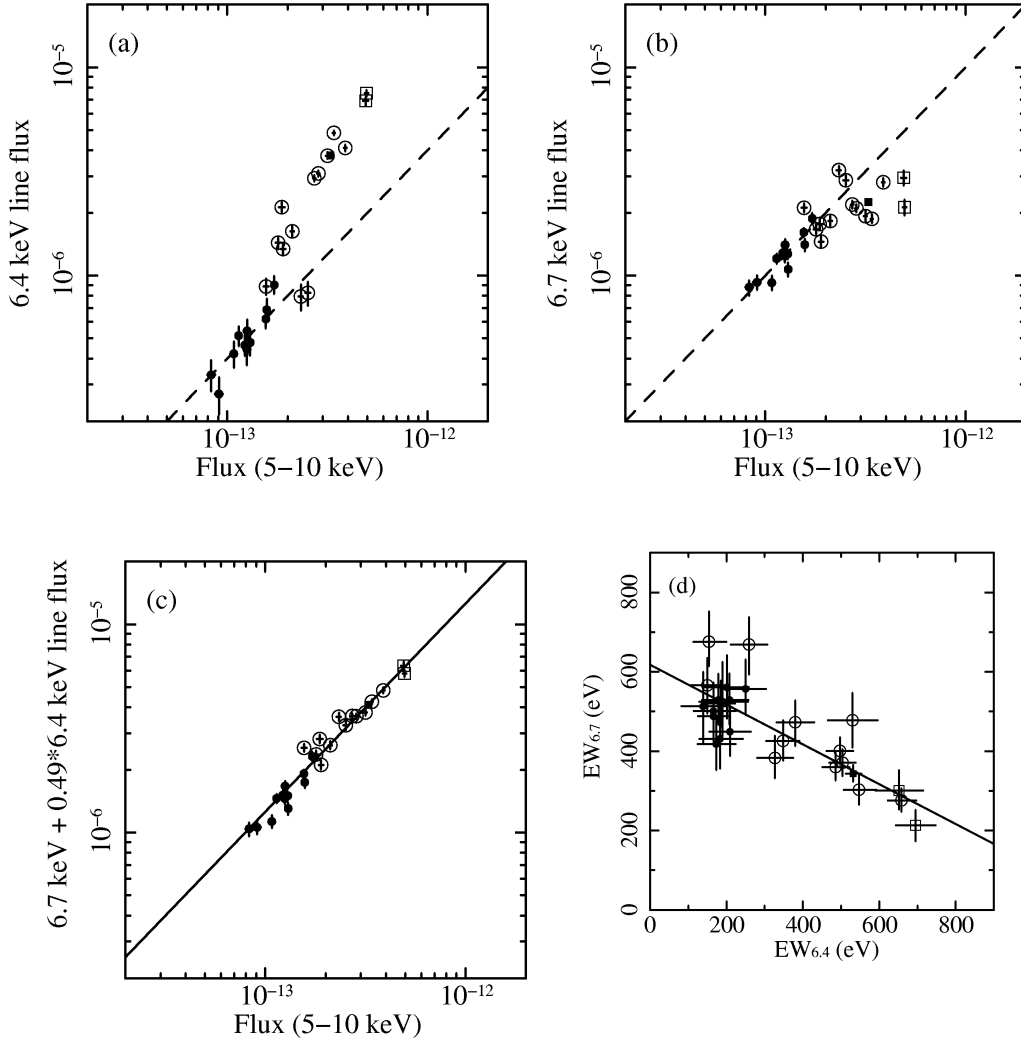


Fig. 2. Correlation plots between the physical parameters. The open and filled circles are data from the east and west fields, respectively. For comparisons, the data of the 6.4 keV clumps (sources 1 and 2) and background are also plotted, as shown by the open and filled squares, respectively (see section 3.2).

a) Plots of the 5–10 keV band flux (L_{5-10} , horizontal axis) vs. the Fe I-K α flux ($F_{6.4}$, vertical axis). The unit of $F_{6.4}$ and L_{5-10} are [$\text{photons cm}^{-2} \text{ s}^{-1} \text{ arcmin}^{-2}$] and [$\text{ergs cm}^{-2} \text{ s}^{-1} \text{ arcmin}^{-2}$], respectively. The dashed line is an eye guide to the proportional relation of $L_{5-10} \propto F_{6.4}$.

b) Same as (a), but for Fe xxv-K α ($F_{6.7}$).

c) Same as (a), but for the sum of the line flux of Fe xxv-K α ($F_{6.7}$) and Fe I-K α ($F_{6.4}$). The solid line is the best-fit proportional line of $F_{6.7} + 0.49 \times F_{6.4} = 1.26 \times 10^7 \times L_{5-10}$.

d) Same as (a), but for the relation of the equivalent width of the Fe xxv-K α line ($EW_{6.7}$) and that the Fe I-K α line ($EW_{6.4}$). The solid line shows the best-fit relation of $EW_{6.7} + 0.50 \times EW_{6.4} = 0.62 \text{ [keV]}$.

6.4 keV ($EW_{6.4}$) and the 6.7 keV ($EW_{6.7}$) lines, we made correlation plots (figure 2). For a consistency check of the best-fit parameters between the east and west fields, we made two spectra from the small region of the overlap of both fields and fitted the spectra with the same model of equation 1. Since this small region includes the calibration Mn I-K α and K β lines at 5.9 and 6.5 keV, the 6.4 keV flux ($F_{6.4}$) is contaminated by the 6.5 keV line. Therefore, we compared the best-fit flux of the 6.7 keV line ($F_{6.7}$) and the power-law in the 5–10 keV band (L_{5-10}). The best-fit values of $F_{6.7}$ are $3.88^{+0.40}_{-0.16}$ and $4.06^{+0.21}_{-0.28}$ (in unit of 10^{-5} photons $\text{cm}^{-2} \text{s}^{-1}$) for the east and west fields, respectively. The best-fit values of L_{5-10} are $3.57^{+0.09}_{-0.09}$ and $3.58^{+0.08}_{-0.09}$ (in unit of 10^{-12} ergs $\text{cm}^{-2} \text{s}^{-1}$) for the east and west fields, respectively. Thus, we confirmed that the relevant best-fit parameters obtained from two fields are consistent with each other.

Figure 2a shows that the flux ratio of the Fe I-K α line ($F_{6.4}$) to the 5–10 keV band (L_{5-10}) is not constant, but $F_{6.4}$ shows excess at larger flux domains. Figure 2b shows a vice versa flux-relation of the Fe XXV-K α line ($F_{6.7}$) to the 5–10 keV band (L_{5-10}). These facts indicate that the 5–10 keV band flux (L_{5-10}) does not solely associate with the Fe I-K α line nor the Fe XXV-K α line.

We therefore searched for a possible combination of the Fe XXV-K α and Fe I-K α flux to become proportional to the 5–10 keV band flux. Figure 2c shows the relation of the combined 6.7 keV and 6.4 keV flux ($F_{6.7}$ and $F_{6.4}$) vs. the 5–10 keV band flux (L_{5-10}). The best-fit relation is

$$F_{6.7} + 0.49(^{+0.03}_{-0.04}) \times F_{6.4} = 1.26 \times 10^7 \times L_{5-10}, \quad (2)$$

where the data dispersion (1σ) from the best-fit relation is 11%. This relation is confirmed by correlation plots of the equivalent width of the Fe XXV-K α line ($EW_{6.7}$) and that of Fe I-K α ($EW_{6.4}$). The solid line in figure 2d is the best-fit relation, given as

$$EW_{6.7} + 0.50(\pm 0.06) \times EW_{6.4} = 0.62(\pm 0.07) \text{ [keV]}. \quad (3)$$

We note that Warwick et al. (2006) reported a similar (but rather qualitative) analysis using the emission lines obtained by XMM-Newton observations.

The correlations of equations 2 and 3 suggest that the power-law component (PL) can be divided into two parts, PL1 and PL2, which are the power-law continuums associated with the K-shell lines from neutral and highly ionized atoms, respectively. We hence divide the 5–10 keV band flux of L_{5-10} to L_{15-10} and L_{25-10} , which belong to PL1 and PL2, respectively. These phenomenological relations of equations 2 and 3 also mean that the flux ratio L_{25-10}/L_{15-10} is proportional to $\sim(1/0.5) \times (F_{6.7}/F_{6.4})$. In figure 3, we plot the photon index (Γ) as a function of the flux ratio of Fe I-K α to Fe XXV-K α ($F_{6.4}/F_{6.7}$). Although the values $F_{6.4}/F_{6.7}$ scatter largely from ~ 0.2 to 4, Γ is almost constant at about 1.9; the continuum shape is the same regardless the line ratio. Therefore, PL1 and PL2 have nearly the same photon indices (Γ) of 1.9.

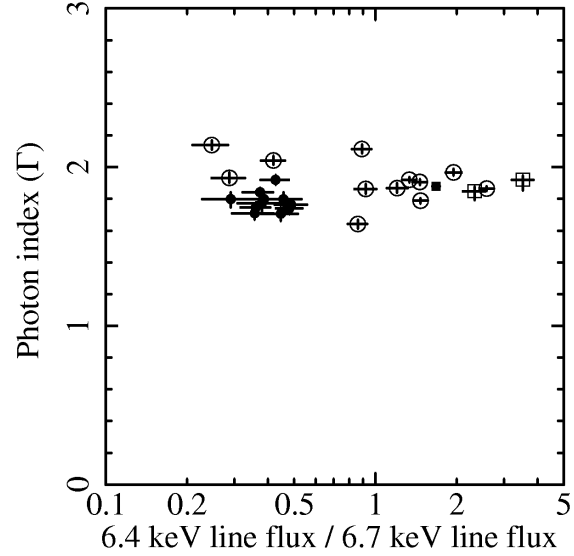


Fig. 3. Same as figure 2, but for the line flux ratio of Fe I-K α and Fe XXV-K α ($F_{6.4}/F_{6.7}$) (horizontal axis) vs. the photon index Γ (vertical axis).

3.2. X-ray Image and Spectra of the 6.4 keV Clumps near the GC

In figure 1, we can see strong enhancements of the 6.4 keV line near at the Radio Arc (sources 1 and 2). To make reliable spectra of sources 1 and 2, a precise estimation of the Galactic center diffuse X-rays (GCDX) is particularly important, because the GCDX comprises the major background, and is variable from position to position (see section 3.1). To minimize any systematic error due to subtraction of the position-dependent GCDX, we selected the background region to be as near as possible to sources 1 and 2. The background region thus selected is shown by the dashed ellipse in figure 1, where the data of sources 1 and 2 (polygons) are excluded.

First, we obtained the source and background spectra, and fitted with a phenomenological model of equation 1. The best-fit fluxes of the Fe XXV-K α lines for sources 1 and 2, and that of the background are $2.95(^{+0.24}_{-0.24}) \times 10^{-6}$, $2.13(^{+0.19}_{-0.18}) \times 10^{-6}$ and $2.25(^{+0.06}_{-0.06}) \times 10^{-6}$ [photons $\text{cm}^{-2} \text{s}^{-1} \text{arcmin}^{-2}$], respectively. Therefore, the GCDX in source 1 would be larger, but that in source 2 is smaller than the GCDX in the background region. Thus, a key issue is how to properly subtract the GCDX. As is suggested in section 3.1, the power-law component (PL) of the GCDX is divided into PL1 and PL2, which are associated with the 6.4 keV (neutral iron) and 6.7 keV (He-like iron) lines, respectively. It is very likely that PL1 and PL2 are also associated with the K-shell lines from neutral and highly ionized atoms. In order to subtract PL2 and associated K-shell lines from highly ionized atoms, we introduced a multiply factor, α , which is the ratio of the 6.7 keV flux ($F_{6.7}$) of source 1 (or 2) to that

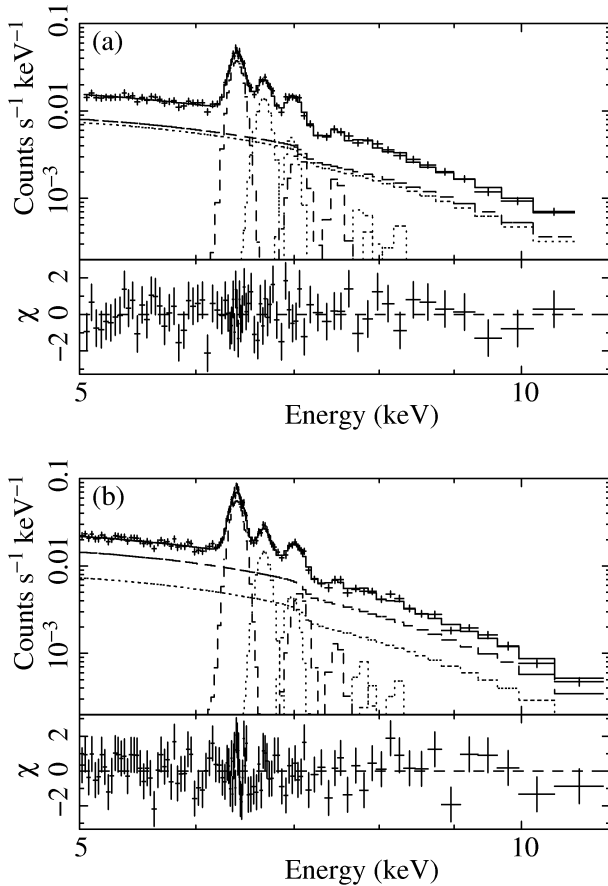


Fig. 4. X-ray spectra of source 1 (a) and source 2 (b). The dashed lines are the best-fit model of the sources, while the dotted lines are the model GCDX spectra obtained by the method given in the text. The CXB spectra are out of the frame of these figures.

of the background spectrum. The factors α are 1.31 for source 1 and 0.95 for source 2. We then re-constructed a background model consisting of the K-shell lines from highly ionized atoms and the relevant continuum component. As for the fluxes of the K-shell lines from highly ionized atoms, we multiplied the factor α to those of the best-fit line-flux of the background spectrum. For the continuum, on the other hand, we multiplied the factor of $\alpha \times F_{6.7}/(F_{6.7} + 0.5 \times F_{6.4})$ to the best-fit PL of the background spectrum, where $F_{6.7}$ and $F_{6.4}$ are the line fluxes of the background regions. This is the same as $\alpha \times \text{PL2}$, where PL2 is that from the background region.

Adding this model background and CXB, we fitted the spectra of sources 1 and 2 with a model of an absorbed power-law plus $K\alpha$ and $K\beta$ lines of neutral iron and nickel. The best-fit spectra are given in figure 4 with the dashed lines together with the model background (dotted line). The best-fit source parameters are listed in table 1. Note that the spectral parameters of sources 1 and 2 include the PL1 components of the background region.

Table 1. Best-fit parameters of the background-subtracted sources.

	source 1	source 2
Ab_{Fe}^*	$3.8^{+0.6}_{-0.5}$	$3.9^{+0.4}_{-0.6}$
Photon index (Γ)	$1.83^{+0.03}_{-0.03}$	$1.86^{+0.03}_{-0.02}$
L_{5-10}^\dagger	$2.61^{+0.14}_{-0.16}$	$3.37^{+0.12}_{-0.12}$
$F_{6.4}^\ddagger$	$6.92^{+0.29}_{-0.30}$	$7.45^{+0.29}_{-0.23}$
$EW_{6.4}^\S$	$1.23^{+0.14}_{-0.14}$	$1.03^{+0.08}_{-0.09}$
$F_{7.05}^\ddagger$	$0.99^{+0.27}_{-0.25}$	$1.02^{+0.19}_{-0.23}$

* Iron abundances determined by the iron K-edge depth with a fixed N_{H} of $6 \times 10^{22} \text{ cm}^{-2}$.

† Unabsorbed 5–10 keV band flux in unit of $10^{-13} \text{ erg s}^{-1} \text{ cm}^{-2} \text{ arcmin}^{-2}$.

‡ Unabsorbed line fluxes of Fe I- $K\alpha$ ($F_{6.4}$) and $K\beta$ ($F_{7.05}$) in unit of $10^{-6} \text{ photons s}^{-1} \text{ cm}^{-2} \text{ arcmin}^{-2}$.

§ Equivalent width of the Fe I- $K\alpha$ line in unit of keV.

3.3. Timing Analysis of the 6.4 keV Clumps near the GC

Muno et al. (2007) reported a time variability of the sub-structures in source 1 in Chandra observations. We therefore extended the time variability study for a longer time scale from the Chandra (2002) to the Suzaku (2005) observations. Since the spatial resolution of Suzaku is limited to resolve the sub-structures in source 1, and since the image position of source 1 with Suzaku and Chandra are slightly shifted from each other, we extracted the X-ray spectra from a larger region than source 1, as is given by the solid ellipses in figure 5. We subtracted the NXBG from the Suzaku spectrum in the same way as previously described, and fitted the spectra with the model of equation 1. The best-fit Suzaku fluxes of the 6.4 and 6.7 keV lines are given in table 2. For the Chandra spectrum, we subtracted the off-plane CXB (including NXBG) data using the “blank-sky” data-sets. The Chandra spectrum was fitted with the same model as Suzaku (equation 1), fixing the line energies, the power-law index and iron K-edge absorption to the Suzaku best-fit values. Free parameters were normalizations (flux) of the power-law and Gaussian lines. For a reasonable fit, we fine-tuned the Chandra energy gain by $\sim 0.2\%$. The best-fit Chandra fluxes of the 6.4 and 6.7 keV lines are listed in table 2.

From table 2, we can see that the 6.7 keV line flux is constant within the 90% level of the statistical errors. This result is reasonable, because the 6.7 keV line is due to the largely extended GCDX, and hence should be invariant on the time scale of a few years. In other words, the constant 6.7 keV flux supports that the over-all systematic flux error of the 6.4 keV and 6.7 keV lines between the Chandra and the Suzaku observations, under the present procedure of data selection, screening and analysis, is smaller than the statistical 1.5σ error. We note that even if the power-law index and iron K-edge absorption are free parameters in the fitting of the Chandra spectrum, the best-fit fluxes have almost the same values as listed in table 2. Thus, from table 2, the flux change of the 6.4 keV line from the Chandra (2002) to the Suzaku (2005) observations is significant at the 4.7σ level (note that the errors in table 2 are at the 90% level).

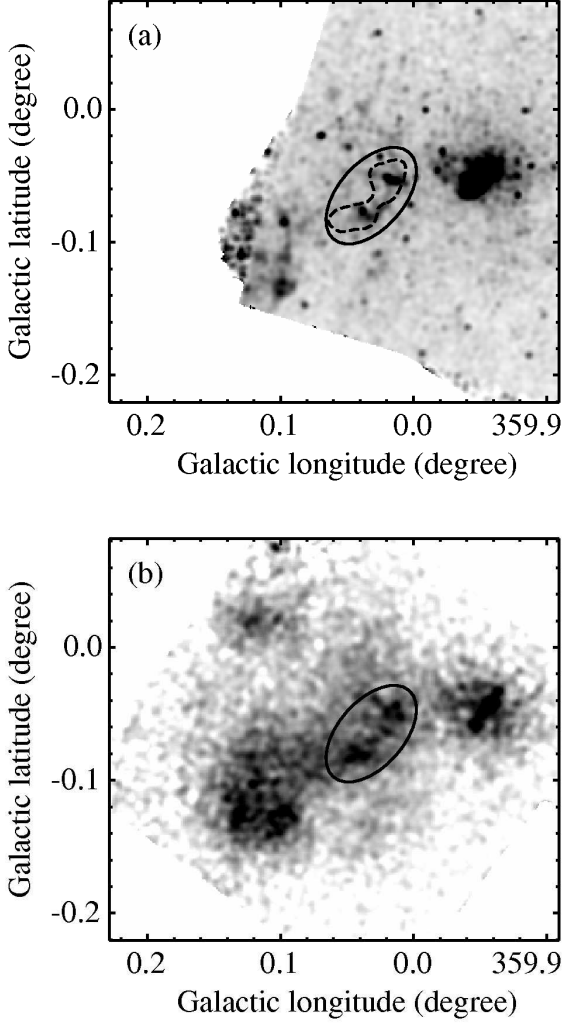


Fig. 5. (a) X-ray image obtained with Chandra in the 6–7 keV band, and (b) the Suzaku image in the 6.4 keV line band (6.32–6.48 keV). The dashed polygon in (a) shows source 1 (see text). The spectra are taken from the solid ellipses in (a) and (b).

Table 2. Best-fit fluxes of the 6.4 and 6.7 keV lines of the Suzaku and Chandra observations.

	Chandra (2002)	Suzaku (2005)
Ab_{Fe}^*	3.4^\dagger	$3.4^{+0.5}_{-0.4}$
Photon index (Γ)	1.77^\dagger	$1.77^{+0.02}_{-0.02}$
$F_{6.4}^\ddagger$	$7.83^{+0.23}_{-0.23}$	$6.89^{+0.20}_{-0.23}$
$F_{6.7}^\ddagger$	$3.37^{+0.20}_{-0.20}$	$3.61^{+0.19}_{-0.18}$

* Iron abundances determined by the iron K-edge depth with a fixed N_{H} of $6 \times 10^{22} \text{ cm}^{-2}$.

† Fe abundance and Γ are fixed to the Suzaku best fit values.

‡ Unabsorbed line fluxes of Fe I-K α and Fe XXV-K α in unit of $10^{-5} \text{ photons s}^{-1} \text{ cm}^{-2}$.

4. Discussion

4.1. Decomposition of the GC Emission

The GCDX would have at least 3 components: high-temperature plasma (component-1), the 6.4 line with Thomson scattering or bremsstrahlung continuum (component-2), and integration of point sources plus other possible origins (component-3). K-shell lines from highly ionized atoms from component-1 constrain the plasma parameters. The most important lines are Fe XXV-K α (the 6.7 keV line), Fe XXVI-K α (the 6.97 keV line) and Fe XXV-K β (the 7.88 keV line). The flux ratio of the 6.97 keV line to the 6.7 keV line gives the ionization temperature, while that of the 7.88 keV line to the 6.7 keV line gives the electron temperature. Koyama et al. (2007d) extensively studied the line flux (and ratio) from the GC (the east and west fields), and concluded that the GCDX has a high-temperature plasma in collisional ionization equilibrium. The GC spectrum was, in fact, nicely fitted with a 6.5 keV plasma and a power-law with a photon index of $\Gamma = 1.4$, plus neutral K-shell lines (see figure 7 in Koyama et al. 2007d). The continuum flux in the 5–10 keV band of the high-temperature plasma was $\sim 0.5 \times L_{5-10}$ of the GCDX (the east and west fields) and that of the power-law ($\Gamma = 1.4$) was $\sim 0.5 \times L_{5-10}$ (see figure 7 in Koyama et al. 2007d).

As we already proposed, we can decompose the 5–10 keV band flux (L_{5-10}) into two components, L_{15-10} and L_{25-10} with the flux ratio L_{25-10}/L_{15-10} being proportional to $(1/0.5) \times (F_{6.4}/F_{6.7})$. Koyama et al. (2007d) found that the mean fluxes of the 6.7 keV line ($F_{6.7}$) and that of the 6.4 keV line ($F_{6.4}$) in the east and west fields are nearly equal to each other (see table 4 and figure 7 in Koyama et al. 2007d). Therefore, for the mean 5–10 keV band flux of the east and west fields, about 2/3 ($1/1.5$) is attributable to the 6.7 keV line and the other 1/3 ($0.5/1.5$) is to the 6.4 keV line. The photon indices (Γ) for the both components are the same at 1.9 (see section 3.1).

The above two decompositions implicitly assumed that the 6.7 keV line is due to a plasma with a spatially uniform temperature. This assumption was verified by a spatial analysis of the flux ratio of Fe XXV-K α (6.7 keV line, $F_{6.7}$) to Fe XXVI-K α (6.97 keV line, $F_{6.97}$). In figure 6, we plot the correlation of $F_{6.97}$ and $F_{6.7}$.

From figure 6, we conclude that the plasma temperatures are approximately uniform. In detail, however, the flux ratios are systematically larger, and hence show a higher temperature in the west field than that in the east field by $\sim 10\%$ (figure 6). Koyama et al. (2007d) reported that the GC has a lower temperature plasma (the soft component) with highly ionized atomic lines, such as silicon and sulfur. We therefore fit the low-energy band spectra, and found the plasma temperature to be ~ 1 keV. The contribution of this plasma to the 6.7 keV-line flux is 5–10%, but those to the 6.96 keV line and the 5–10 keV flux are negligible. The flux shift of the 6.7 keV line is within the 1σ dispersion of the line flux vs. the continuum flux correlation (figure 2c). Including these effects increases the temperature by $\sim 5\%$. Using the K-edge

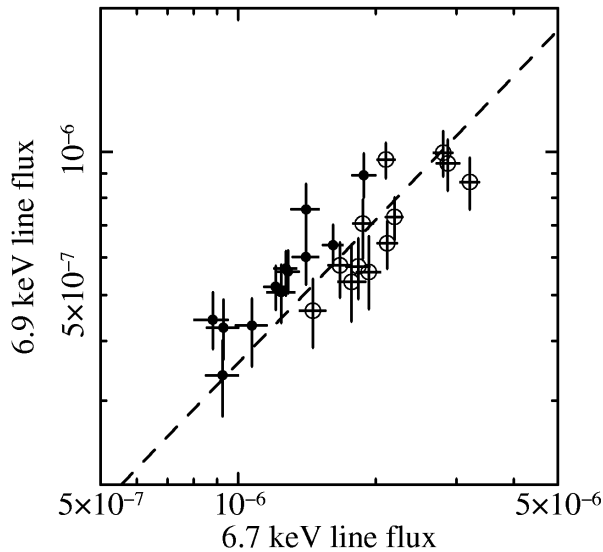


Fig. 6. Same as figure 2, but the line flux plots of Fe XXVI-K α ($F_{6.97}$) (horizontal axis) and Fe XXV-K α ($F_{6.7}$) (vertical axis).

structure, Koyama et al. (2007d) determined that the line-of-sight N_{Fe} to the GCDX is $9.7 \times 10^{18} \text{ cm}^{-2}$. This corresponds to a 3.5 solar abundance of iron, assuming that the N_{H} to the GCDX is $6 \times 10^{22} \text{ cm}^{-2}$. However the assumed N_{H} of $6 \times 10^{22} \text{ cm}^{-2}$ may be smaller than the typical values. In fact, the Suzaku observations on the Sgr A East (SNR) and Arches (star cluster) revealed that N_{H} is $9\text{--}14 \times 10^{22}$ (Koyama et al. 2007c; Tsujimoto et al. 2007). Then, the iron K-edge abundance determined by the K-edge absorption is reduced to be 2.3–1.5 solar. On the other hand, the iron abundances of the 6.5 keV plasma in the GCDX were determined to be ~ 1 solar by Koyama et al. (2007d). Warwick et al. (2006) also reported that the iron abundance in the GCDX plasma is one solar. The 1 keV plasma is associated with the 2.46 keV line. Nobukawa et al. (2008) and Mori et al. (2008) analyzed some of the 2.46 keV clumps, and found that the abundances of iron and other heavy elements are consistent with solar. Thus, iron abundance in the 1 keV plasma is likely to be one solar, and hence the $F_{6.7}$ values and the temperatures may not be significantly changed. We can therefore ignore the 1 keV plasma in the discussion.

Now, we schematically show the results of the two different decompositions of the 5–10 keV band flux (L_{5-10}) in figure 7. The right side shows nearly equal participation of the 6.5 keV plasma (parenthesis is a phenomenological photon index), and the power-law with $\Gamma = 1.4$ (Koyama et al. 2007d). The 6.4 keV line was treated separately, and hence is not included in figure 7 (right). The left side shows the phenomenological participations in this work, PL1 and PL2 with a flux ratio of 1:2. The 6.7 keV and 6.4 keV lines are mainly included in the white and grey regions, respectively. There is an apparent discrepancy

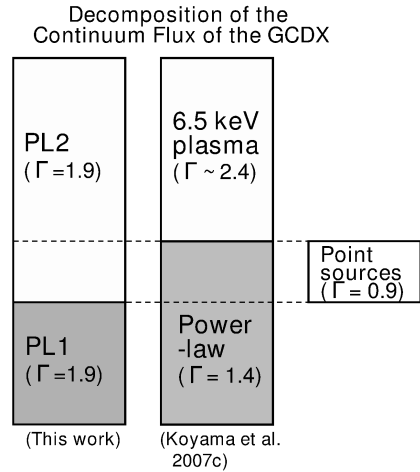


Fig. 7. Schematic picture of the continuum flux (L_{5-10}) participation of the GCDX. The right side shows nearly equal participation of the 6.5 keV plasma (parenthesis is a phenomenological photon index), and the power-law $\Gamma = 1.4$ (Koyama et al. 2007d). The left side shows the phenomenological participations (PL1 and PL2 with a ratio of 1:2). White and grey indicates the region of the power-law, which exhibits mainly the 6.7 keV and 6.4 keV lines, respectively.

between the two decompositions. This may be solved if we take a point-source contribution into account (see the next section).

4.2. Origin of the High Temperature Plasma

The spectral analysis of the GC (the east and west fields) indicates that about half of the GCDX is due to the 6.5 keV plasma, which emits the 6.7 keV line and other K-shell lines from highly ionized iron and nickel (Koyama et al. 2007d). However, figure 7 suggests that, additionally, at least 1/6 of the total GCDX should also be the 6.7 keV line emitter. We propose that this is integrated point sources (component-3), because Muno et al. (2004) reported that similar fractions of the GCDX come from point sources of $\geq 3 \times 10^{-15} \text{ ergs cm}^{-2} \text{ s}^{-1}$ (2–9 keV), and the spectrum has a strong 6.7 keV line and a rather weak 6.4 keV line (see figure 7 of Muno et al. 2004). Therefore, in the present analysis, PL2 (the left of figure 7) may be contaminated by the integrated flux of point sources. On the other hand, in the analysis of Koyama et al. (2007d), the 6.7 keV line from the point sources would be implicitly included in the 6.5 keV plasma (the right), while the continuum component of the point sources is included in the power-law component of $\Gamma = 1.4$. The continuum shape of the 6.5 keV plasma is approximated by a power-law of $\Gamma = 2.4$, while the integrated point sources has 0.9 (Muno et al. 2004). Then, the flux-weighted mean value is $\Gamma \sim 2.0$, consistent with $\Gamma = 1.9$ of PL2. The power-law of $\Gamma = 1.4$ component is regarded as a sum of the PL1 ($\Gamma = 1.9$) and the point sources of $\Gamma = 0.9$. Then, the weighted mean photon index of the power-law component becomes $\Gamma \sim 1.6$, consistent with $\Gamma = 1.4$.

From the above analysis, we infer that $\sim 1/6$ of the GCDX is due to point sources that are already resolved by Chandra down to the flux 3×10^{-15} erg cm $^{-2}$ s $^{-1}$. Since point sources fainter than this flux level must be prevailing in the GC, the fraction of point source contribution to the GCDX of $1/6$ is the lower limit. Revnivtsev et al. (2006), Revnivtsev & Sazonov (2007) and Revnivtsev et al. (2007) proposed that the point-source population contributes largely to the Galactic ridge diffuse X-rays (GRDX). This scenario may also be applied to the GCDX. The point-source distribution should be symmetric with respect to Sgr A*. However, we found the east-west asymmetry of the 6.7 keV line flux ($F_{6.7}$) as demonstrated by the open (east) and filled (west) circles in figure 2b (also see figure 6 of Koyama et al. 2007d). The mean flux in the east field is ~ 1.5 times larger than that of the west field. As we already pointed out, the 1-keV temperature plasma can not account for such a large asymmetry (see section 4.1). Thus, the maximum possible contribution of the point sources to the GCDX is about 70% for the east region and 100% for the west field. In this case, however, the spectrum of the integrated point sources must have, approximately, a power-law with $\Gamma=1.9$ (or 17 keV temperature plasma) with sizeable 6.4 keV and 6.7 keV lines ($EW_{6.4} = 150\text{--}700$ eV, $EW_{6.7} = 200\text{--}800$ eV) and the line ratio $F_{6.97}/F_{6.7}=0.3\text{--}0.4$. As far as we know, the most probable and popular point sources having such a hard spectrum with sizeable 6.4, 6.7 and 6.96 keV lines are intermediate poplars (IP). Ezuka & Ishida (1999) compiled 14 ASCA data-sets of 12 IPs. The mean $EW_{6.4}$ and $EW_{6.7}$ are 140 eV and 220 eV, respectively (calculated from table 2 of Ezuka & Ishida 1999), which are systematically smaller than those in the GCDX (see figure 2d). Thus, it may be unlikely that a large fraction of the GCDX can be accounted for by such point sources. At this moment, however, we reserve any definite conclusion until more quantitative estimates and observations for both the point source and the diffuse emission are evaluated.

4.3. Origin of the 6.4 keV-line and the Clumps

The origin of the 6.4 keV emission is due to the inner-shell ionization of nearly neutral irons. A plausible source for the inner-shell ionization is bombarding on the cloud gas by either high-energy electrons or high-energy X-rays. The former produces a relatively weak equivalent width of the 6.4 keV line ($EW_{6.4}$) of ~ 0.3 keV (e.g. Tatischeff 2003), compared to the latter case of $EW_{6.4} \sim 1$ keV (for the solar abundance of iron) (e.g. Murakami et al. 2000). In section 3.1, we show that the K-shell lines from neutral atoms and associated continuum (PL1) are prevailing in the GCDX. Substituting $EW_{6.7} = 0$ in equation 3, we obtain $EW_{6.4} = 1.4$ keV in PL1. Also, from the discussion in section 3.1, we can say that Γ for PL1 is ~ 1.9 . As is noted in section 3.2, the spectral parameters of sources 1 and 2 (table 1) include the PL1 components in the background region. However, the best-fit $EW_{6.4} = 1.0\text{--}1.2$ keV (table 1) and power-law index $\Gamma = 1.8$ are almost identical to those from PL1 in the background region. Hence, no essential change on the spectral parameters (table 1), other

than reducing the absolute fluxes, is present.

The spectra of source 1 and source 2 were studied with Chandra and XMM-Newton (Yusef-Zadeh et al. 2002, Predehl et al. 2003, Yusef-Zadeh et al. 2007). However the best-fit $EW_{6.4}$ were scattered from observation to observation. This may be due to GCDX subtraction, because GCDX is variable from position to position. In fact, the results of the off-plane background subtraction, where $F_{6.7}$, and hence L_{25-10} , is smaller than those in the source region, give systematically smaller $EW_{6.4}$ compared to that of the near-by background subtraction. We argue that the present results of the $EW_{6.4} \sim 1.0\text{--}1.2$ keV are reliable, because the GCDX is taken from a nearby background, and possible spatial variations of the GCDX are best estimated (see section 3.1). The $EW_{6.4}$ value of $\sim 1.0\text{--}1.2$ keV is consistent with that irradiated by X-rays, unless the iron abundance in the east and west fields is $\sim 4\text{--}5$ times solar. Although we have no conclusive data for the iron abundance in the cold cloud, the iron abundance in the GCDX is likely to be ~ 1 solar (see section 4.1). Therefore, the observed equivalent width of the 6.4 keV line in sources 1 and 2 may favor, if not be conclusive, the origin of X-ray irradiation, rather than electron bombarding.

The iron K-edge (N_H) depth at 7.1 keV is another key parameter to judge the origin of the 6.4 keV clumps. If the N_H values are far larger than that of the Galactic absorption toward the GC, then the electron origin may not be favored (see Tatischeff 2003). The N_H value is, however, sensitive to the NXBG subtraction, because it becomes significant at high energy above ~ 7 keV. Since Suzaku has low and stable NXBG compared to those of Chandra and XMM-Newton (Koyama et al. 2007a), we argue that the present result of $N_H \sim 2 \times 10^{23}$ (assuming 1 solar abundance of iron) is more reliable. This value is somehow larger than that toward the general GC regions (see section 4.1), but still may not be conclusive to judge whether the origin is X-rays or electrons.

The most direct evidence to favor the X-ray origin is the time variability of the clumps, as was reported by Munro et al. (2007) for the sub-structures of source 1. Also, the time variability of Sgr B2, the other 6.4 keV clump, was found by Koyama et al. (2008). We further confirmed the time variability of source 1 from the Chandra (2002) to the Suzaku (2005) observations with a $5\text{-}\sigma$ confidence level. The real scale of source 1 is a few light-years, and hence the 3-year time variability of source 1 is possible only when the physical information travels across the source as fast as the speed of light, like X-ray irradiation. This speed is impossible by electrons and/or any finite-mass particles.

The authors thank all of the Suzaku team members, especially H. Uchiyama, H. Nakajima, H. Yamaguchi, and H. Mori for their support and useful information on the XIS performance. This work is supported by Grant-in-Aids from the Ministry of Education, Culture, Sports, Science and Technology (MEXT) of Japan, the 21st Century COE "Center for Diversity and Universality in Physics", Scientific Research A (KK),

Priority Research Areas in Japan “New Development in Black Hole Astronomy”(TGT), and Grant-in-Aid for Young Scientists B (HM). HM is also supported by the Sumitomo Foundation, Grant for Basic Science Research Projects, 071251, 2007. TI and YH are supported by JSPS Research Fellowship for Young Scientists.

References

- Ezuka, H., & Ishida, M. 1999, *ApJS*, 120, 277
- Koyama, K., Awaki, H., Kunieda, H., Takano, S., & Tawara, Y. 1989, *Nature*, 339, 603
- Koyama, K., Maeda, Y., Sonobe, T., Takeshima, T., Tanaka, Y., & Yamauchi, S. 1996, *PASJ*, 48, 249
- Koyama, K., et al. 2007a, *PASJ*, 59, S23
- Koyama, K., et al. 2007b, *PASJ*, 59, S221
- Koyama, K., Uchiyama, H., Hyodo, Y., Matsumoto, H., Tsuru, T. G., Ozaki, M., Maeda, Y., & Murakami, H. 2007c, *PASJ*, 59, 237
- Koyama, K., et al. 2007d, *PASJ*, 59, S245
- Koyama, K., Inui, T., Matsumoto, H. & Tsuru, T. 2008, *PASJ*, 60, S201
- Mitsuda, K., et al. 2007, *PASJ*, 59, S1
- Mori, H., Tsuru, T. G., Hyodo, Y., Koyama, K., & Senda, A. 2008, *PASJ*, 60, S183
- Muno, M. P., et al. 2004, *ApJ*, 613, 326
- Muno, M. P., Baganoff, F. K., Brandt, W. N., Park, S., & Morris, M. R. 2007, *ApJ*, 656, L69
- Murakami, H., Koyama, K., Sakano, M., Tsujimoto, M., & Maeda, Y. 2000, *ApJ*, 534, 283
- Murakami, H., Koyama, K., & Maeda, Y. 2001, *ApJ*, 558, 687
- Nobukawa, M., et al. 2008, *PASJ*, 60, S191
- Predehl, P., Costantini, E., Hasinger, G., & Tanaka, Y. 2003, *Astronomische Nachrichten*, 324, 73
- Reid, M. J. 1993, *ARA&A*, 31, 345
- Revnivtsev, M., Sazonov, S., Gilfanov, M., Churazov, E., & Sunyaev, R. 2006, *A&A*, 452, 169
- Revnivtsev, M., & Sazonov, S. 2007, *A&A*, 471, 159
- Revnivtsev, M., Vikhlinin, A., & Sazonov, S. 2007, *A&A*, 473, 857
- Serlemitsos, P. J., et al. 2007, *PASJ*, 59, S9
- Tatischeff, V. 2003, *EAS Publications Series*, 7, 79 ([astro-ph/0208397v1](#))
- Tsujimoto, M., Hyodo, Y. & Koyama, K. 2007, *PASJ*, 59, S229
- Yusef-Zadeh, F., Law, C., & Wardle, M. 2002, *ApJ*, 568, L121
- Yusef-Zadeh, F., Muno, M., Wardle, M., & Lis, D. C. 2007, *ApJ*, 656, 847
- Wang, Q. D., Dong, H., & Lang, C. 2006, *MNRAS*, 371, 38
- Warwick, R., Sakano, M., & Decourchelle, A. 2006, *Journal of Physics Conference Series*, 54, 103